Structure–Function Analysis of the Acyl Carrier Protein Synthase (AcpS) from Mycobacterium tuberculosis

ARTICLE *in* JOURNAL OF MOLECULAR BIOLOGY · OCTOBER 2009

Impact Factor: 4.33 · DOI: 10.1016/j.jmb.2009.08.065 · Source: PubMed

doi:10.1016/j.jmb.2009.08.065 J. Mol. Biol. (2009) 393, 937–950

JMB

Available online at www.sciencedirect.com

ScienceDirect

ELSEVIER

Structure–Function Analysis of the Acyl Carrier Protein Synthase (AcpS) from *Mycobacterium tuberculosis*

Orly Dym[1,2]*, Shira Albeck[1,2], Yoav Peleg[1,2], Alon Schwarz[1], Zippora Shakked[1], Yigal Burstein[3] and Oren Zimhony[4]*

[1]*Department of Structural Biology, Weizmann Institute of Science, Rehovot 76100, Israel*

[2]*Israel Structural Proteomics Center, Weizmann Institute of Science, Rehovot 76100, Israel*

[3]*Department of Organic Chemistry, Weizmann Institute of Science, Rehovot 76100, Israel*

[4]*Kaplan Medical Center, affiliated to the Hebrew University, Rehovot 76100, Israel*

Received 8 July 2009; received in revised form 25 August 2009; accepted 28 August 2009
Available online
3 September 2009

We have solved the crystal structure of the acyl carrier protein synthase (AcpS) from *Mycobacterium tuberculosis* (*Mtb*) at 1.95 Å resolution. AcpS, a 4-phosphopantetheinyl transferase, activates two distinct acyl carrier proteins (ACPs) that are present in fatty acid synthase (FAS) systems FAS-I and FAS-II, the ACP-I domain and the mycobacterial ACP-II protein (ACPM), respectively. *Mtb*, the causal agent of tuberculosis (TB), and all other members of the Corynebacterineae family are unique in possessing both FAS systems to produce and to elongate fatty acids to mycolic acids, the hallmark of mycobacterial cell wall. Various steps in this process are prime targets for first-line anti-TB agents. A comparison of the *Mtb* AcpS structure determined here with those of other AcpS proteins revealed unique structural features in *Mtb* AcpS, namely, the presence of an elongated helix followed by a flexible loop and a moderately electronegative surface unlike the positive surface common to other AcpSs. A structure-based sequence comparison between AcpS and its ACP substrates from various species demonstrated that the proteins of the Corynebacterineae family display high sequence conservation, forming a segregated subgroup of AcpS and ACPs. Analysis of the putative interactions between AcpS and ACPM from *Mtb*, based on a comparison with the complex structure from *Bacillus subtilis*, showed that the *Mtb* AcpS and ACPM lack the electrostatic complementarity observed in *B. subtilis*. Taken together, the common characteristic of the Corynebacterineae family is likely reflected in the participation of different residues and interactions used for binding the *Mtb* AcpS to ACP-I and ACPM. The distinct features and essentiality of AcpS, as well as the mode of interaction with ACPM and ACP-I in *Mtb*, could be exploited for the design of AcpS inhibitors, which, similarly to other inhibitors of fatty acid synthesis, are expected to be effective anti-TB-specific drugs.

Edited by K. Morikawa

Keywords: structure of acyl carrier protein synthase (AcpS); tuberculosis

Introduction

Tuberculosis (TB) caused by *Mycobacterium tuberculosis* (*Mtb*) claims the lives of millions each year, infecting one individual every second, with one-third of the world's population already infected with *Mtb*. As the emergence of drug-resistant TB is a serious threat for disease control, new drug development is a major focus in the 'Stop TB strategy' supported by the World Health Organization.[1] Fatty acid synthesis is an essential process for cell survival and is particularly proficient and complex for mycobacteria and related species that produce mycolic acids. The mycolate-containing cell wall

**Corresponding authors.* E-mail addresses: Orly.Dym@weizmann.ac.il; oren_z@clalit.org.il.

Abbreviations used: AcpS, acyl carrier protein synthase; *Mtb*, *Mycobacterium tuberculosis*; ACP, acyl carrier protein; FAS, fatty acid synthase; ACPM, mycobacterial ACP-II protein; TB, tuberculosis; CoA, coenzyme A; P-pant, 4′-phosphatepantetheinyl; PPT, phosphopantetheine transferase; PDB, Protein Data Bank; SeMet, selenomethionine; MAD, multiple anomalous dispersion.

plays a role in virulence and drug resistance.[2,3] Various steps in the synthesis of mycolates are targets for first-line anti-TB agents.[4] Mycobacteria and the related bacteria—*Corynebacterium*, *Nocardia*, and *Rhodococcus*—that belong to the Corynebacterineae family[5] are unique among prokaryotes in possessing both fatty acid synthase (FAS)-I and FAS-II systems.[4] The multifunctional, multi-domain FAS-I protein, typically found in parasites, fungi, and all higher eukaryotes, is composed of a single polypeptide chain (α) in both mycobacteria[6] and mammals[7] and two polypeptide subunits (α and β) in fungi.[6,8] The FAS-II, on the other hand, which is found in most prokaryotes and plants, is composed of discrete, monofunctional enzymes.[9] Mycobacterial FAS-I generates and elongates long-chain (C16:0–26:0) acyl-coenzyme A (CoA) derivatives that serve as the precursors for the syntheses of polyketides and of C56:0 meromycolate by FAS-II.[10,11] The elongated acyl intermediates throughout fatty acid synthesis are attached to an acyl carrier protein (ACP). The ACP is a discrete protein of the FAS-II system (ACP-II) or a domain within the multifunctional FAS-I (ACP-I). ACP, which interacts with many protein partners, is an essential protein, as it is critical for the function of other metabolic pathways including the synthesis of polyketide antibiotics, non-ribosomal peptides, and intermediates used in the synthesis of vitamins such as lipoic acid and biotin.[12,13] The inactive apo-form of ACP is converted to the functional holo-form by the covalent attachment of a 4′-phosphatepantetheinyl (P-pant) moiety of CoA to a conserved serine residue on the apo-ACP.[14] The incorporation of P-pant into the ACP-I domain or into the discrete ACP-II protein is carried out by a phosphopantetheine transferase (PPT). The PPT enzymes have been classified based on sequence and structural features into three classes, PPT-I, PPT-II, and PPT-III.[15] The group I PPTs are usually referred to as acyl carrier protein synthases (AcpSs), which are about 120 amino acid residues in length, and display a biologically active trimeric arrangement of α/β fold.[16,17] Group II PPTs are exemplified by the surfactin synthetase-activating enzyme Sfp, which activates the peptidyl carrier protein and exhibits a broad acceptor substrate specificity compared with the AcpS enzyme.[18–20] Sfp is a monomer of about 240 residues, whose structure displays a two-domain composition with intrinsic pseudo-2-fold symmetry, each with similar domain architecture as a single monomer of the trimeric AcpS. The active site is situated in a cleft formed by the two domains.[19,20] The third member of the PPT family consists of PPTs that are an integral part of fungal FAS-I[21–23] and activate the ACP-I domain.[22,24–26]

Two genes encoding PPTases were identified in the genome of *Mtb* H37Rv and related species, encoding AcpS and PptT (belonging to type I and type II classes of PPT, respectively). Both genes were found to be essential for the viability of mycobacterium, thus signifying AcpS from *Mtb* as a potential drug target.[27] AcpS of the Corynebacterineae family activates both the ACP-I domain and the mycobacterial ACP-II protein (ACPM).[27]

We have solved the crystal structure of AcpS from *Mtb* at 1.95 Å resolution and performed a structure-based sequence comparison with other known AcpSs[16,17] and their ACP substrates from different species.[21,22,28–33] In the Corynebacterineae family of bacteria, we found that the AcpS, ACP-II, and ACP-I proteins form a segregated subgroup based on their high sequence conservation. Such conservation likely reflects the common function of this family of bacteria in using the FAS-I and FAS-II systems, each activated by a common AcpS. We show that the electrostatic complementarity between the *Mtb* AcpS and ACPM is much less pronounced than that of *Bacillus subtilis*, thus suggesting that different residues, utilizing different interactions, are likely to play a role in the binding of the *Mtb* AcpS and ACPM.

Results and Discussion

Structural overview of AcpS

We have solved the crystal structure of *Mtb* AcpS, which crystallized with one monomer per asymmetric unit [Protein Data Bank (PDB) code: 3HQJ]. The tightly packed functional AcpS trimer was generated using the 3-fold crystallographic symmetry in the *P*23 space group (Fig. 1a). The trimeric structure observed in the crystal is consistent with the apparent molecular weight of the AcpS complex, as determined based on gel-filtration chromatography. The structure of the AcpS monomer, characterized by an α/β fold similar to that of other AcpS enzymes,[16,17] includes three significant structural motifs. The first is a classical three-stranded antiparallel β-sheet formed by strands β1↓, β5↑, and β4↓ (Fig. 1b). A long α-helix, α3, packs diagonally against the β-sheet and, together with α-helices α1, α2, η1, and α4 of the antiparallel four-helical bundle, forms the second structural motif. The third feature consists of a two-stranded antiparallel β-sheet (β2 and β3). In the trimeric complex, the three-stranded antiparallel β-sheets of each AcpS monomer are arranged together in a barrel-like structure, forming a long, mostly hydrophobic channel that runs through the structure. The α3 helix in *Mtb* AcpS structure is extended compared to other AcpSs, and the loop connecting α3 to η1 is considerably elongated, adopting an 'open' conformation (Fig. 1a). The extended α3 helix positions the open loop of one monomer close to the loop connecting β2 to β3 of the neighboring monomer. The *Mtb* AcpS trimer is stabilized by the interactions between residues from β4 (situated at the N terminus of one monomer) and β1 (situated at the C terminus of the neighboring monomer), as well as by multiple interactions between residues from the extended α3 and the open loop of one monomer and those of the loop

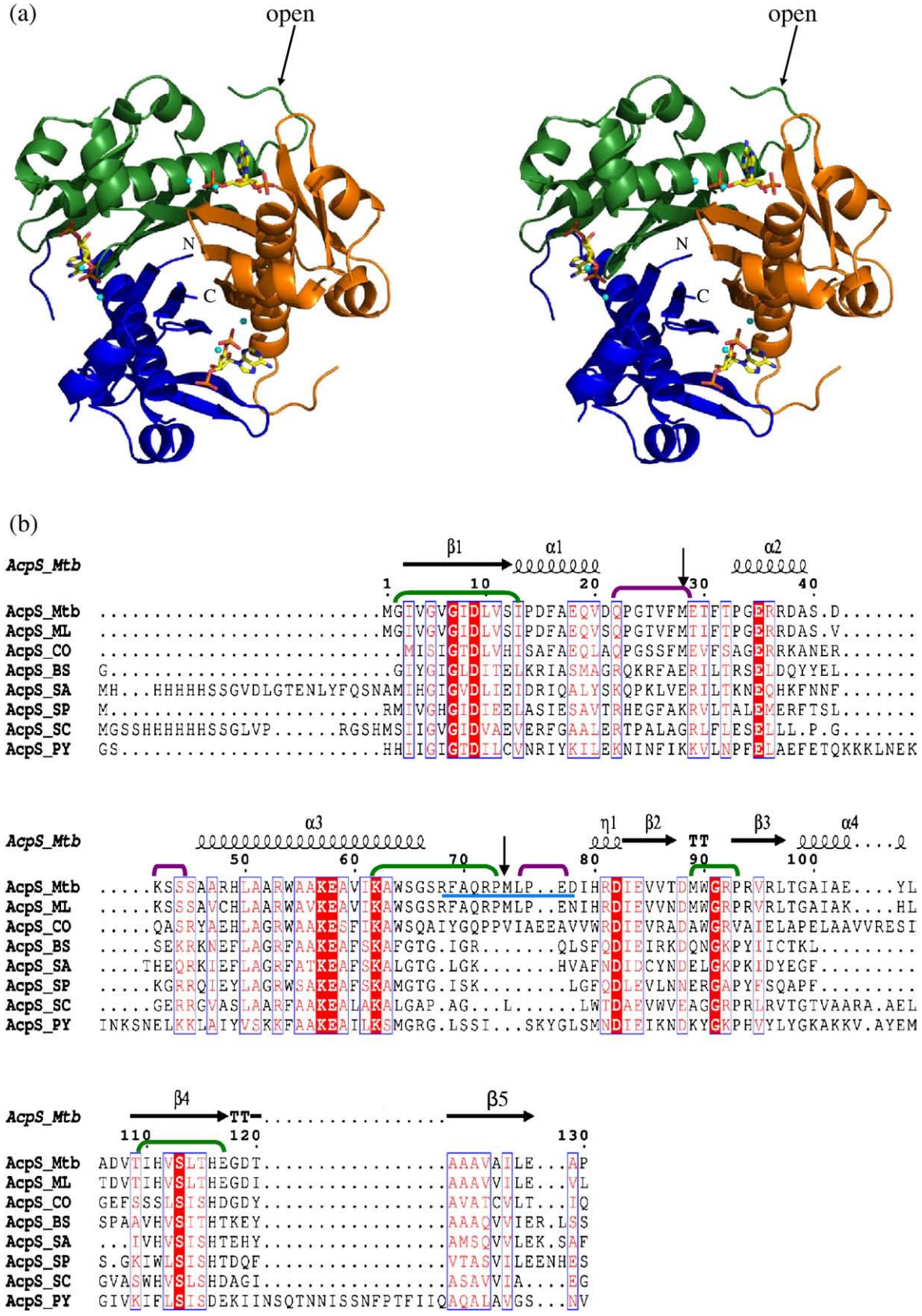

Fig. 1 (*legend on next page*)

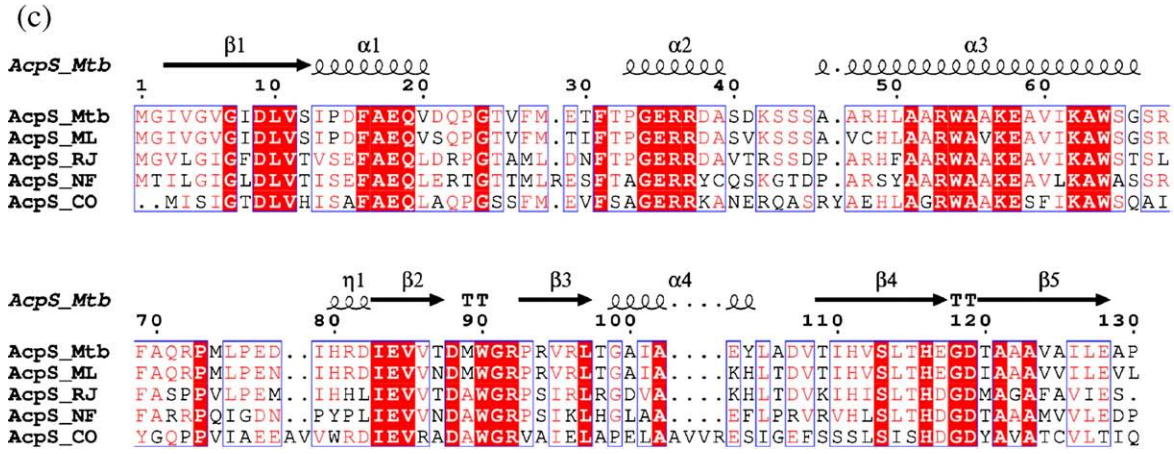

Fig. 1. (a) Ribbon stereoview representation of the *Mtb* AcpS trimer structure (in green, blue, and orange) (residues 2–130). The Mg atoms are shown as cyan balls. The 3′,5′-ADP moieties of the CoA, drawn as sticks (yellow for C, red for O, and blue for N), are situated in the cleft between each of two monomers forming three active sites per AcpS trimer. (b) Structure-based sequence alignment of AcpS proteins from *M. tuberculosis* (AcpS_Mtb, PDB code: 3HQJ), *M. leprae* (AcpS_ML), *C. glutamicum* (AcpS_CO), *B. subtilis* (AcpS_BS, PDB code: 1F7T), *S. aureus* (AcpS_SA, PDB code: 3F09), *S. pneumoniae* (AcpS_SP, PDB code: 1FTH), *S. coelicolor* (AcpS_SC, PDB code: 2JBZ), and *P. yoelii* (AcpS_PY, PDB code: 2QG8). All α-helices are depicted by spirals and labeled above the corresponding sequence. The residues conserved in all proteins are highlighted in red, and similar residues appear in blue boxes. The introduced Met mutations are labeled by black arrows; residues for which no electron density is observed are labeled with a purple line, and residues involved in monomer–monomer interactions are labeled with a green line. The elongated α3 helix and extended loop are indicated by a blue line. (c) Structure-based sequence alignment of the AcpSs from the Corynebacterineae family of bacteria subgroup. *Mtb* (AcpS_Mtb), *M. leprae* (AcpS_ML), *R. jostii* (AcpS_RJ), *N. farcinica* (AcpS_NF), and *C. glutamicum* (AcpS_CO) exhibit a high sequence identity. Numbering and secondary elements are presented according to the structure of AcpS_Mtb. The sequence-based alignments were produced using TCoffee,[34] and the figure was created using ESPript.[35]

between β2 and β3 of the adjacent monomer, forming a tight trimer (Fig. 1b). The active site containing CoA is situated in a cleft formed between two adjacent monomers, such that each pair of adjacent monomers of AcpS contributes to the formation of an active site resulting in three active sites (Fig. 1a).

Segregation of the AcpS, ACP-I, and ACP-II proteins of the Corynebacterineae family of bacteria

A low sequence identity exists between *Mtb* AcpS and other AcpS proteins (ranging from 18% to 25%) (Fig. 1b). However, in comparison with the enzymes from other members of the Corynebacterineae family of bacteria, the *Mtb* AcpS exhibits a high sequence identity (*Mycobacterium leprae*, 87.7%; *Corynebacteriumglutamicum*, 43.8%; *Rhodococcusjostii*, 63.1%; and *Nocardia farcinica*, 55%), as illustrated by the multiple sequence alignment shown in Fig. 1c. Thus, we suggest that the AcpS expressed by the Corynebacterineae family of bacteria comprises a distinct subgroup having the structural features described here. Besides their sequence homology, the AcpS species of this subgroup are distinct proteins, rather than an integral domain of the FAS-I polypeptide chain (as in the case of fungi).[22,23] Moreover, whereas AcpS from other species activate a single ACP substrate (either the ACP-I domain of FAS-I or the ACP-II protein of FAS-II), the AcpS molecules from the Corynebacterineae family have a dual functionality—activating ACP from both systems.[22]

The ACP-II proteins generally exhibit low sequence conservation among species (only 6 residues, Fig. 2a). The ACP-II proteins from the Corynebacterineae family of bacteria, however, exhibit relatively high conservation (25 residues) (Fig. 2b). Thus, similar to AcpS (Fig. 1c), the ACP-II proteins from this family of bacteria also segregate to a subgroup displaying high sequence conservation.

The ACP-I domain and the ACP-II protein are only weakly related, as evidenced by the insignificant sequence similarity between them, with only the active Ser41 being strictly conserved. Moreover, ACP-I is about twice as large as ACP-II, such that its N-terminal region forms the core domain and its C-terminal region is defined as the additional domain. Therefore, in the absence of an *Mtb* FAS-I structure, identifying the ACP-I domain was difficult. We therefore used the known sequence and structure of the yeast ACP-I domain (PDB code: 2PFF and 2UV8)[21,22] to identify the *Mtb* ACP-I domain (residues 1770–1850 constitute its core domain and residues 1851–1935 make up its additional domain).

Interestingly, although high sequence conservation is found among the members of the Corynebacterineae family (25 conserved residues), only 7 residues are strictly conserved among other ACP-I of the FAS-I family members (see Supplementary Fig. 1a and b, respectively). In conclusion, the finding that AcpS, ACP-II, and ACP-I of the

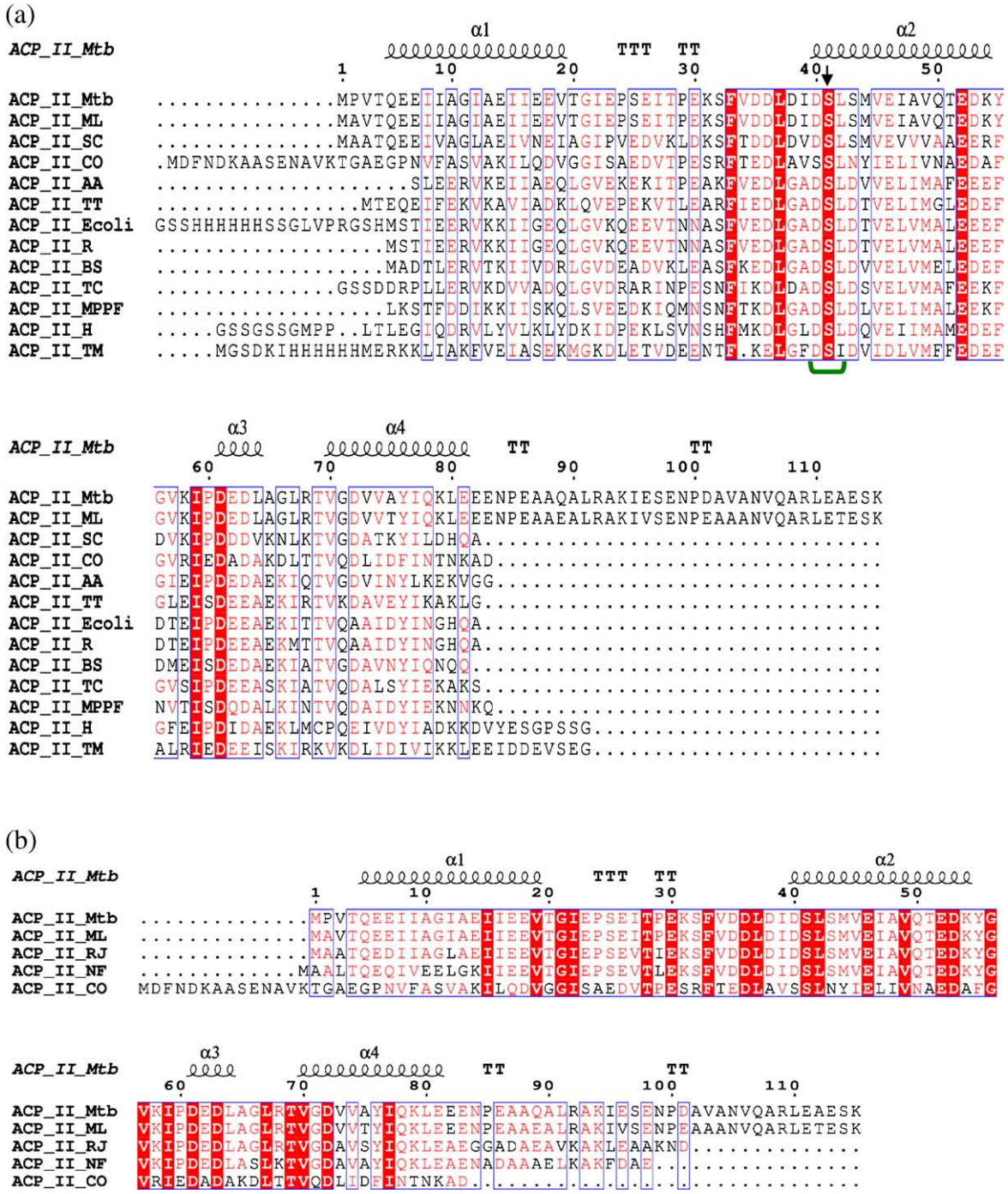

Fig. 2. Structure-based sequence alignment of ACP-II from different species. (a) *M. tuberculosis* (ACP_II_Mtb, PDB code: 1KLP), *M. leprae* (ACP_II_ML), *S. coelicolor* (ACP_II_SC, PDB code: 2CNR), *C. glutamicum* (ACP_II_CO), *Aquifex aeolicus* (ACP_II_AA, PDB code: 2EHS), *Thermus thermophilus* (ACP_II_TT, PDB code: 1X3O), *E. coli* (ACP_II_Ecoli, PDB code: 1ACP), cyclic AMP-specific phosphodiesterase from rat (AMP_II_R, PDB code: 1LOI), *B. subtilis* (ACP_II_BS, PDB code: 1HY8), *Toxoplasma gondii* apicoplast (ACP_II_TC, PDB code: 2QNW), malaria parasite *Plasmodium falciparum* (ACP_II_MPPF, PDB code: 2FQ0), human (ACP_II_H, PDB code: 2DNW), and *Thermotoga maritima* (ACP_II_TM, PDB code: 1VKU) are presented. (b) The ACP-II from the Corynebacterineae family of bacteria, *Mtb* (ACP_II_Mtb), *M. leprae* (ACP_II_ML), *R. jostii* (ACP_II_RJ), *N. farcinica* (ACP_II_NF), and *C. glutamicum* (ACP_II_CO), exhibit a high sequence identity. Numbering and secondary elements are presented according to the structure of *Mtb* ACP. The figure was generated as for Fig. 1b and c.

Corynebacterineae family of bacteria appear to form a segregated subgroup likely reflects the common function of this family of bacteria using both FAS-I and FAS-II systems that are activated by a common AcpS. This finding is consistent with a study of protein interaction networks in *Escherichia coli* that

described a particularly large divergence for ACP and its interacting proteins for different orders of bacteria, including the Actinobacteridea, to which the Corynebacterineae family belongs.[9]

Structural comparison of *Mtb* AcpS with other PPT family members

AcpS belongs to group I PPT family, for which 3D structures are available for the following species: *B. subtilis* (AcpS_BS), PDB code: 1F7T;[16] *Streptococcus pneumoniae* (AcpS_SP), PDB code: 1FTH;[17] *Streptomyces coelicolor* (AcpS_SC), PDB code: 2JBZ; *Staphylococcus aureus* (AcpS_SA), PDB code: 3F09; and *Plasmodium yoelii* (AcpS_PY), PDB code: 2QG8. Despite the low sequence identity between *Mtb* AcpS and the different AcpS proteins (an average of 25%), the *Mtb* AcpS displays a similar fold to the other family members, as evidenced by the low pairwise rmsds among them (an average of 1.5 Å). An analysis of the residues involved in *Mtb* AcpS trimer formation revealed that the following residues contribute to the interface between each pair of adjacent monomers: Ile3, Val6, Ile8, and Leu10 of β1 and His111, Ser113, Leu114, Thr115, and Glu117 of β4 (green frames in Fig. 1b). Interestingly, although the residues in these positions are also involved in trimer formation of the AcpS from the other species, certain residues (Val6 and His111) are not strictly conserved, suggesting that the conservation is on the structural position of these residues and not necessarily on their identity.

The overlaid structures of the AcpS proteins show that the *Mtb* AcpS structure is similar to that of other proteins belonging to group I PPT, with the notable exception of the extended α3 helix and its subsequent loop connecting α3 to η1 (residues 68–77) (Fig. 3a and b). The extended α3 positions the loop closer to the neighboring monomer, adopting an open conformation (Fig. 3b). This open conformation allows residues from the open loop of one monomer to interact with residues from the loop connecting β2 to β3 (residues 88–92) of the neighboring monomer, forming a tight trimer. In contrast, in the other AcpS structures of this group, the α3 helix is considerably shorter and it positions the subsequent loop in a 'closed' conformation, thereby sequestering it from the neighboring

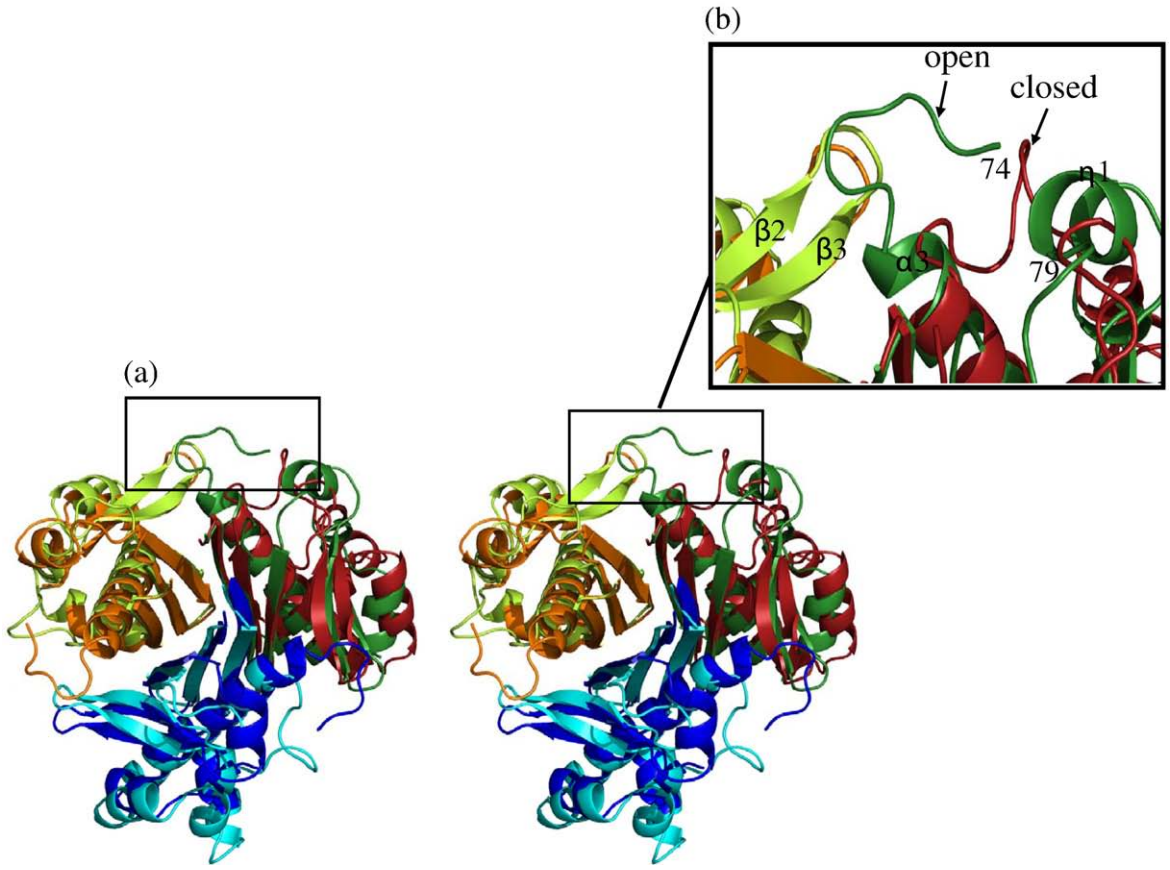

Fig. 3. (a) Stereoview of the overlaid structures of the *Mtb* AcpS trimer (green, blue, and orange) and the *B. subtilis* trimer (red, cyan, and lemon). (b) Closer view of the open and closed conformations of *Mtb* and *B. subtilis* AcpSs, respectively (box of Fig. 3a). The extended α3 helix of *Mtb* AcpS positions the open loop between α3 and η1 of one monomer (green) closer to the loop connecting β2 to β3 of the neighboring monomer (orange). The shorter α3 of *B. subtilis* AcpS positions the loop connecting α3 to η1 of one monomer (red) in a closed conformation, such that it is sequestered from the neighboring monomer (lemon).

monomer (Fig. 3b). The finding that residues 75–78, which are part of the open loop, did not exhibit electron density suggests that this loop is flexible. Moreover, many of the residues in this loop are non-conserved among the AcpSs (Fig. 1b). Notably, in the structure of the AcpS–ACP complex from *B. subtilis* (PDB code: 1F80), the residues from the closed loop are involved in multiple interactions with both ACP residues and with the P-pant moiety. Thus, we suggest that residues from this loop may be involved in the specific recognition of its ACP partners. Certain residues in the interacting loops (Asp88, Trp90, Arg92, Ser65, Phe69, Gln71, and Pro73) are strictly conserved only among the AcpS species from bacteria belonging to the Corynebacterineae family (Fig. 1c). Based on the sequence similarity of the α3 helix from AcpSs belonging to this family, we can reasonably assume that the other members will exhibit an extended α3 and an open loop conformation as well. Thus, the open conformation of this loop and its flexibility appear to be properties that could be related to the unique function of the AcpS proteins from the Corynebacterineae family of bacteria; namely, their ability to interact with both ACP-I and ACP-II. We can reasonably assume that in the presence of ACP, this loop will be stabilized.

A DALI[36] search revealed a structural similarity to two other, more distantly related proteins belonging to the group II PPT [*B. subtilis* Sfp (PDB code: 1QR0)[20] and the *Homo sapiens* PPT (PDB code: 2BYD)] and one member of the group III PPT family [the PPT domain of the FAS-I from yeast (PDB code: 2PFF)].[21,22] The type II PPT proteins display a two-domain structure, with an intrinsic pseudo-2-fold symmetry, each with similar domain architectures as a single monomer of the *Mtb* AcpS. All three PPT family groups display very low amino acid conservation, as only seven residues are conserved (Gly7, Asp9, Glu35, Lys57, Glu58, Lys62, and Asp82). These strictly conserved residues all have defined roles; two of the invariant residues, Glu35 and Lys57, participate in a conserved intramolecular salt bridge present in all known AcpS structures. This salt bridge was shown to be essential in the restriction of the mobility of a conserved hydrophobic residue in position Trp/Phe54, which, in turn, was shown to create a hydrophobic pocket for the P-pant arm (in certain cases when present).[16] Other strictly conserved residues include Lys62, Asp9, and Glu58, all having a primary role in CoA binding and ACP activation. Thus, PPT types I, II, and III exhibit evolutionary conservation of the AcpS fold, whereas sequence conservation is limited to the several functional residues that are involved in CoA binding.

The interaction of *Mtb* AcpS with CoA

The structure of *Mtb* AcpS incorporates Mg atoms and 3′,5′-ADP, both situated in a cleft formed by two monomers of AcpS (Fig. 1a). Although *Mtb* AcpS was co-crystallized in the presence of CoA, only the 3′,5′-ADP moiety, the hydrolysis product of CoA, exhibits a well-defined electron density, whereas the P-pant moiety of CoA has no continuous and defined electron density. This finding suggests that either this moiety is very flexible and therefore disordered in the crystal structure or that it is released to the solution immediately following catalysis. Since we observed noncontinuous electron density that can be assigned to the β-phosphate of the P-pant arm, the P-pant is likely to be present but disordered in this structure. The flexibility of the P-pant arm is a common phenomenon among other PPT family members for which no electron density has been observed in the corresponding crystal structures.[20] Moreover, in the AcpS structures that do exhibit a well-defined electron density for the P-pant arm, the interactions with the protein are weak and predominately of a van der Waals nature, involving residues from the extended α3 and the loop connecting α3 to η1.[16,37] In the *Mtb* AcpS structure, these residues are part of the open loop and are situated far away from the P-pant, thereby leaving this moiety nonrestricted.

The interactions between the 3′,5′-ADP moiety and protein residues at the active-site pocket are predominantly hydrogen bonds involving mostly conserved residues from the extended α3 of one monomer and residues from β4 and the loop between β2 and β3 of the neighboring monomer (Figs. 1b and 4a). The adenine moiety is involved only in two van der Waals contacts to Arg92 and to the conserved Pro93 from one monomer and a hydrogen bond with Ser65 situated at the extended part of the α3 helix of the adjacent monomer. The two phosphate groups of the 3′,5′-ADP moiety, the 3′-phosphate (P3) of the adenine ribose and the α-phosphate (Pα), are bound tightly to the protein by multiple hydrogen bonds. The two conserved basic residues, Arg53 and Lys62, play a key role by forming salt bridges each to two oxygen atoms of the P3 and Pα phosphates, respectively. The α-phosphate is also coordinated to water molecules and to two magnesium atoms. In fact, a continuous electron density is observed for these magnesium atoms at the active site of *Mtb* AcpS (Fig. 4b). Each of the magnesium atoms has a six-coordination sphere. Thus, one of the magnesium atoms (Mg2) interacts with oxygen O3 of the α-phosphate, ND1, and main-chain oxygen of His116 from one monomer and three water molecules. The other magnesium atom (Mg1) is complexed with oxygen O1 of the α-phosphate, the conserved Asp9 residue from the adjacent monomer, and four water molecules. One of the latter water molecules is within hydrogen-bond distance to the conserved Glu58 residue. A similar coordination, in which the α-phosphate is bound to two magnesium atoms, has been observed only for AcpS from *P. yoelii* (PDB code: 2QG8), whereas the α-phosphate is bound to one magnesium atom (Mg1) in the rest of the known AcpS structures. In these structures, the magnesium is also coordinated to at least two water molecules and to a

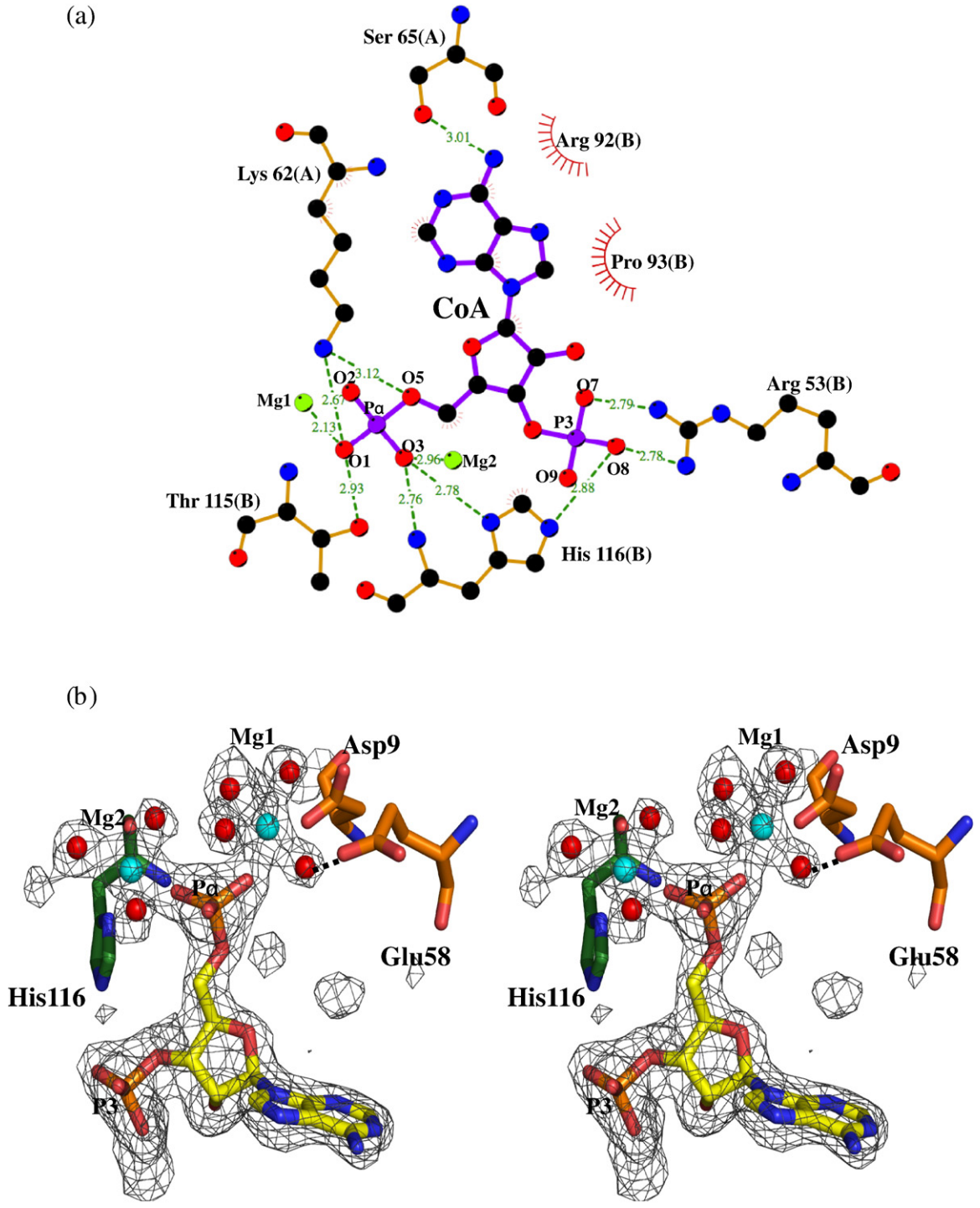

Fig. 4. The active site of *Mtb* AcpS. (a) LIGPLOT[38] presentation of the AcpS residues interacting with the 3′,5′-ADP moiety of CoA. The residues, from two adjacent monomers (labeled A and B) that form hydrogen bonds and salt bridges to the ligand, are labeled and are shown in ball-and-stick representation. The two phosphate groups of the ligand are labeled as P3 and Pα, and the two magnesium atoms (Mg1 and Mg2) are shown as green balls. Hydrogen bonds are presented as green broken lines, and the interatomic distances are shown in angstroms. The residues that form van der Waals contacts with the 3′,5′-ADP are depicted as labeled arcs. (b) Electron density map ($F_{obs}-F_{calc}$) contoured at 2σ, where the 3′,5′-ADP moiety, the magnesium atoms, and water molecules were omitted. The ligand atoms are shown as sticks, and the magnesium atoms and water molecules are shown as cyan and red balls, respectively. The protein residues, Glu58, Asp9 of one monomer, and His116 of the neighboring monomer, are shown as sticks.

strictly conserved Asp9 residue. In some of these structures, the magnesium is also complexed to the conserved Glu58 residue (AcpS_BS, PDB code: 1F7L;[16] AcpS_PY, PDB code: 2QG8) or to the β-phosphate (AcpS_SC, PDB code: 2JBZ). Interestingly, in the proteins belonging to the group II PPT (*B.*

subtilis Sfp, PDB code: 1QR0,[20] and the *H. sapiens* PPT, PDB code: 2C43),[37] the magnesium atom is coordinated to a water ligand, to Glu58 and Asp9 residues, and to the α and β groups of the pyrophosphate. Glu58, which is one of the few strictly conserved residues among all AcpS proteins (Fig. 1b), has been proposed to have an important role in the reaction mechanism of activation of ACP by PPT from group II.[37] According to this mechanism, Glu58 abstracts the proton from ACP-Ser41-hydroxyl, converting it into a nucleophile that attacks the β-phosphate of CoA, thereby initiating P-pant transfer to Ser41. A different mechanism was proposed for the AcpS from the group I family, where the metal-bound, activated water molecule removes the hydrogen from the Ser41-hydroxyl group of ACP. Based on this mechanism, it would be possible for AcpS to hydrolyze CoA to P-pant and 3′,5′-ADP in the absence of ACP.[16]

In the *Mtb* AcpS structure, the conserved Glu58 residue is not directly coordinated to the magnesium atom (Mg1) but rather to a metal-bound water molecule. In fact, the side chain of Glu58 is pointing away from the magnesium atom; therefore, it is not likely to be involved in deprotonation of the Ser41-hydroxyl group of ACP, as was proposed for the PPT group II family.[37] One of the three metal-bound water molecules could possibly be involved in the removal of the hydrogen from active Ser, as was suggested for the AcpS from the group I PPT family.[16] Alternatively, the unique presence of two magnesium atoms bound to the α-phosphate as observed in the *Mtb* AcpS structure and its dual functionality—activating ACP from both FAS-I and FAS-II systems—could suggest yet a different mechanism. Further studies of the 3D structure of the AcpS–ACPM complex and AcpS–ACP domain of FAS-I could shed light on the catalytic mechanism.

The putative interactions between *Mtb* AcpS and ACPM

Two structures of complexes between AcpS and ACP, from *B. subtilis* (group I PPT family) (PDB code: 1F80)[16] and from human (group II PPT family) (PDB code: 2CG5),[37] have been published. Both *Mtb* and *B. subtilis* AcpSs belong to the group I PPT family; therefore, structure analysis of the known complex structure of *B. subtilis* AcpS and its ACP[16] could shed light on this interaction in *Mtb*. The *B. subtilis* complex structure contains 35 contacts (up to 3.5 Å), predominantly of electrostatic nature, that are contributed by 9 residues from ACP and 10 residues from AcpS. The key AcpS residues Arg15, Arg22, Arg29, and Arg72 of *B. subtilis* are involved in salt bridges with acidic residues from ACP. Arg15 forms a network of interactions involving a salt bridge with Asp40 (part of the DSL motif green brackets in Fig. 2a) and a hydrogen bond with Asp43 of ACP (Fig. 5a). These complementary interactions serve to position the ACP molecule so that one end of its α2 helix is placed at the bottom of the active site and correctly orients the active Ser41.[16] Arg15 is conserved in most AcpS proteins, yet in the Corynebacterineae family, this amino acid is often substituted by an acidic residue (Asp15, Figs. 1c and 5a). Consequently, this network of interactions is predicted to be lost. The second important basic residue of the *B. subtilis* AcpS is Arg22, which forms a salt bridge with Glu46 from ACP. This basic residue is conserved among all the AcpS proteins, except in *Mtb*, in which it is substituted by Gln, thereby eliminating this salt bridge as well. The third basic residue, Arg29 of AcpS, which forms a salt bridge with Glu52 from ACP, is substituted by Glu29 in *Mtb* AcpS. Therefore, this residue is also expected not to be involved in this complementary interaction. In *B. subtilis*, Arg72 of AcpS is within hydrogen-bond distance to Glu63 from ACP. Although conserved in *Mtb* AcpS, Arg72 is situated on the open loop and is therefore most likely to be too far to interact with Glu63. These four basic residues of *B. subtilis* AcpS generate an electropositive patch on the surface of the protein (Fig. 5b), which interacts with the electronegative surface of *B. subtilis* ACP. Electrostatic calculation revealed that *Mtb* AcpS, on the other hand, lacks this electropositive patch and actually displays an electronegative nature (Fig. 5c). In addition, the *Mtb* ACPM structure (PDB code: 1KLP) displays a considerably lower overall negative charge.[33] Thus, the electrostatic complementarity between the two *Mtb* proteins is much less pronounced than in the AcpS and ACP complex from *B. subtilis*.

A different interaction of AcpS and ACP was observed for the human PPT–ACP complex (PDB code: 2CG5), in which the structure reveals that the two proteins comprise large interfaces, which are mostly hydrophobic.[37] The human ACP active site is situated in a cleft formed by the two domains of the PPT.[19,20] The interactions between human PPT and its ACP substrate involve three hydrophobic patches composed of 7 residues from the ACP mostly situated on the α2 helix. Although 5 of these residues are conserved with the *Mtb* ACP (Ile20, Leu37, Leu42, Met44, and Val45), only 1 (Trp54) out of the 13 residues from the human PPT that are involved in these hydrophobic patches is conserved with the *Mtb* AcpS.[37] Interestingly, although residues from the α2 helix of *B. subtilis* ACP are also responsible for binding AcpS, the type of recognition is clearly different.[16] Highly conserved, negatively charged residues of *B. subtilis* ACP mediate binding to the AcpS, whereas the complex formation in the human is mainly stabilized by hydrophobic interactions.[37] Thus, *Mtb* AcpS and ACPM share very few conserved residues that are involved in AcpS and ACP complex formation with their corresponding proteins from either *B. subtilis* or human; therefore, it is reasonable to assume that different interactions, possibly hydrophobic, involving different residues from human PPT, will play a role in *Mtb* AcpS–ACPM complex recognition.

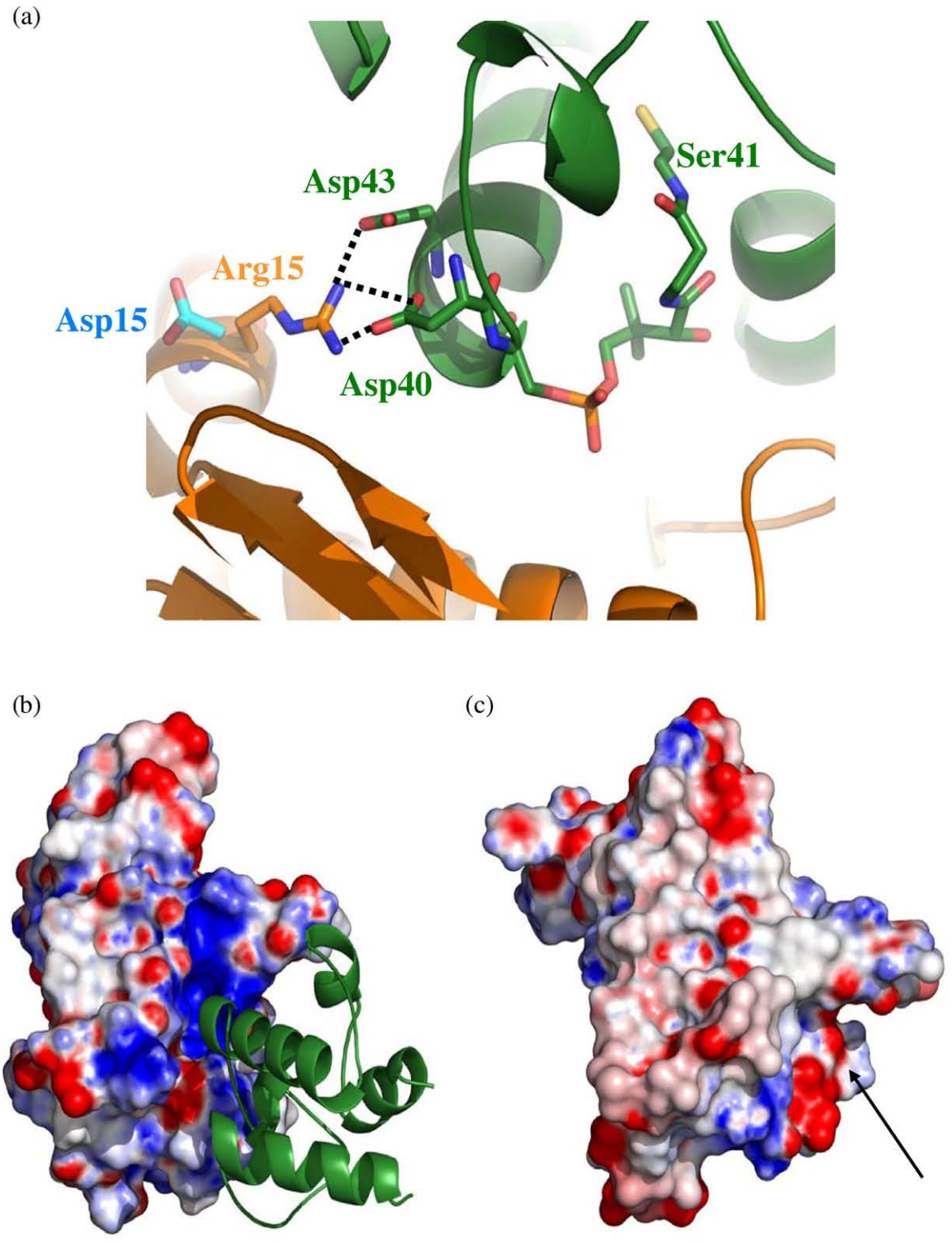

Fig. 5. (a) Salt-bridge contacts formed between *B. subtilis* AcpS (orange) and ACP (green) observed in the complex structure (PDB code: 1F80). The Arg15 in AcpS forms a salt bridge with Asp35 and is within hydrogen-bond distance to Asp38 of ACP (Fig. 2). This Arg is conserved in most AcpS proteins; in the Corynebacterineae family of bacteria, however, this Arg is often substituted by an acidic residue (Asp15). Therefore, this salt bridge does not exist in the complex between *Mtb* AcpS and ACPM. (b) Electrostatic representation of the electropositive surface of *B. subtilis* AcpS with ribbon presentation of the ACP shown in green. (c) Electrostatic representation of *Mtb* AcpS surface using the same orientation as (b), demonstrating a moderate electronegative nature in the putative ACP binding surface indicated by a black arrow.

Summary and Conclusions

Sequence-based structure analysis of AcpS and its ACP substrates from different species revealed that for the Corynebacterineae family of bacteria, AcpS, ACP-I, and ACPM each display high sequence conservation that sets them apart from other bacteria, fungi, and parasites. The segregation of these bacteria is not surprising in view of their unique feature in possessing both FAS-I and FAS-II systems. Structure analysis of *Mtb* AcpS in comparison with the structure of other P-pant transferases revealed several notable differences: a unique extended helix, α3, followed by a flexible loop, connecting α3 to η1, adopting an open conformation. The flexible nature of this loop could explain the unique ability of *Mtb* AcpS to accommodate different substrates, including the ACPM protein of FAS-II and ACP-I, an integral domain of FAS-I. The second structural difference involves the mode of interaction of *Mtb* AcpS with its ACP substrates. Whereas the interactions between AcpS and ACP-II in *B. subtilis* involve multiple salt bridges, the interaction between *Mtb* AcpS and ACPM is expected to rely on different types of interactions due to the marginal electrostatic complementarity between the two partners.

Furthermore, the ACPM is considered to be a promiscuous protein that interacts with multiple protein partners.[13] The ACPM must undergo reversible conformational changes to alternately sequester and release its covalently attached acyl moiety at the active site of its partner enzymes. Such alternation is consistent with the structure of ACPM, which exhibits an inherent flexibility and dynamic conformation. For the FAS-I systems, however, the function of the ACP-I domain probably differs, as it must shuttle among the active sites of neighboring catalytic domains while anchored within a limited space of the FAS-I complex. Therefore, AcpS activation of both ACP protein and domain would require a different mode of accessibility as reflected by the loss of the conserved salt bridges and electrostatic interactions described above. Further studies determining the 3D structure of the ACPM and FAS-I ACP domain in complex with AcpS may further clarify the nature of these interactions.

The observed unique structural features of *Mtb* AcpS and the implied unique mode of interaction with ACPM and FAS-I could be exploited for the design of inhibitors of mycobacterial AcpS, which is an essential protein for *Mtb* viability.[27] In fact, novel anthranilic acid inhibitors of AcpS were identified using high-throughput screening and modeling based on the available *B. subtilis* AcpS structure.[16,39,40] Two compounds were tested against several bacterial species and against the yeast *Candida albicans*, demonstrating variable efficacy.[40] The inhibition of AcpS function *in vivo* should have a profound effect on mycolic acid synthesis and cell wall formation, and hence, similarly to other inhibitors of fatty acid synthesis, such agents can be expected to be highly efficacious against *Mtb*.[4]

Materials and Methods

Expression and purification of *Mtb* AcpS

A 430-bp PCR product containing the *acpS* gene was amplified. *Mtb* AcpS protein (amino acids 2–130 in pACYCDuet-1) containing two mutations A28M and V74M [to enable the use of selenomethionine (SeMet) in the crystal structure determination, see below] was produced with an N-terminal 6× His tag. *E. coli* BL21 (DE3) bacteria expressing His-*Mtb*-AcpS (2–130) were grown at 37 °C in M9 minimal medium containing glucose (0.4 w/v) and chloramphenicol (34 mg/ml). When the cultures reached $A_{600}=0.6$, the following nutrients were added as solids for each 1-l culture: SeMet (50 mg), along with lysine hydrochloride (100 mg), threonine (100 mg), phenylalanine (100 mg), leucine (50 mg), isoleucine (50 mg), and valine (50 mg). Protein expression was induced with 100 μM IPTG at 30 °C overnight. The bacteria were lysed by sonication in 50 mM Tris–HCl, pH 8, 500 mM NaCl, 20 mM imidazole, 1 mM DTT, 1 mM PMSF, protease inhibitor cocktail (Calbiochem), DNaseI (1 μg/ml), and lysozyme (40 U/ml culture). Soluble protein was purified using a Ni-NTA column (HiTrap chelating HP, GE Healthcare) followed by gel-filtration chromatography (HiLoad 16/60 Superdex 75 prep grade, GE Healthcare) in 50 mM Tris, pH 8, 0.1 M NaCl, and 1 mM DTT. Fractions containing *Mtb* AcpS migrating as a trimer were then pooled and applied to an ion-exchange column (Tricorn Q 10/100GL, GE Healthcare) equilibrated with 50 mM Tris, pH 8. The column was eluted with a gradient containing the above buffer and 1 M NaCl. Finally, 1 mM CoA was added to the pooled protein fractions, eluted with 100 mM NaCl, and the protein with its tag was concentrated to 28 mg/ml for crystallization experiments.

Crystallization, data collection, and refinement

The apo crystals of WT *Mtb* AcpS obtained under oil by the microbatch method using the Oryx6 robot (Douglas Instruments Ltd., East Garston, Hungerford, Berkshire, UK) diffracted at best to 3.5 Å resolution. Attempts to solve the WT AcpS structure using the available known structures of AcpS from different species as a starting model for molecular replacement were unsuccessful. We therefore attempted structure determination by multiple anomalous dispersion (MAD) of SeMet. The WT construct used has only a single methionine residue (at position 89), which may not be sufficient for MAD experiments. Therefore, we introduced two additional Met mutations (Ala28Met and Val74Met) based on sequence homology to the highly similar AcpS from *M. leprae*.[32] The presence of these methionine residues in *M. leprae* AcpS suggested that Met replacement at these locations was likely to yield a relevant active protein.[32] Crystals of the SeMet mutant obtained by the sitting drop vapor diffusion method using the Mosquito robot (TTP LabTech Inc, Cambridge, MA, USA) diffracted to 1.95 Å. The SeMet crystals obtained in the presence of 1 mM CoA were grown from a solution of 100 mM $MgCl_2$, 50 mM Na cacodylate (pH 6.5), and 25% polyethylene glycol 200. The crystals formed in the cubic space group $P23$ with cell constants $a=b=c=77.44$ Å and contained one monomer in the asymmetric unit cell with a V_m of 2.72 $Å^3$/Da. A complete data set up to 1.95 Å was collected on a Rigaku R-AXIS IV+ imaging plate area detector mounted on a Rigaku RU-H3R generator with CuKα radiation focused by Osmic confocal mirrors. The

Table 1. Summary of data collection from crystals of SeMet-AcpS

Data collection	
Resolution range (Å)[a]	50.0–1.95 (2.02–1.95)
Space group	*P*23
Unit cell dimensions	
$a=b=c$ (Å)	77.44
Number of molecules in the asymmetric unit	1
Number of reflections measured	156,752
Number of unique reflections[a]	11,568 (1120)
R_{sym}[a,b]	0.08 (0.39)
Completeness (%)[a]	99.9 (100.0)
Redundancy	13.6 (13.2)
$\langle I\rangle/\langle\sigma(I)\rangle$	37.0 (5.6)
Refinement statistics	
Resolution limits (Å)	50.0–1.95
R_{work} (%)[c]	25.2
R_{free} (%)[c]	20.9
Wilson mean *B*-factor (Å^2)	24.95
rmsd (Å)	0.017
Bond angles (°)	1.7
Torsion angles (°)	6.05
Ramachandran plot (%)	
Most favored	95.7
Additional favored	4.3
Generously allowed	0.0
Disallowed regions	0.0

[a] Values in parentheses correspond to the highest-resolution shell.
[b] $R_{sym}=\sum|\langle I_{hkl}\rangle-I_{hkl}|/I_{hkl}|$, where $\langle I_{hkl}\rangle$ is the average intensity of symmetry-related reflections and I_{hkl} is the observed intensity.
[c] $R=\sum||F_{obs}|-|F_{calc}||/\sum|F_{obs}|$, where F_{obs} denotes the observed structure factor amplitude and F_{calc} denotes the calculated one.

diffraction data were indexed and integrated using the program HKL2000.[41] Integrated intensities were scaled using the program SCALEPACK.[41] The structure factor amplitudes were calculated using TRUNCATE from the CCP4 program suite.[42] Using the data thus obtained, we were fortuitously able to solve the AcpS structure by molecular replacement using the known structure of AcpS from *B. subtilis* (PDB code: 1F7T)[16] as a starting model without the need for a SeMet MAD experiment. The refinement was carried out using the program CCP4/Refmac5.[43] The model was rebuilt on the basis of the electron density maps ($2F_{obs}-F_{calc}$ and $F_{obs}-F_{calc}$) using the program Coot.[44] Water molecules were built into peaks greater than 3 σ in the $F_{obs}-F_{calc}$ maps. Although AcpS co-crystallized with CoA, only the 3′,5′-ADP moiety of CoA, a product of the AcpS reaction, exhibited a well-defined electron density. The final refined structure comprised residues 2–130, three magnesium atoms, and 40 water molecules. The regions encompassed by residues 22–29, 41–44, and 75–78 did not exhibit a well-defined electron density (purple lines in Fig. 1b). Electron density was observed only for one of the introduced Met mutations at position 74, whereas the second Met28 mutation was within one of the flexible regions (black arrows in Fig. 1b). The R_{work} value was 20.9% for all data to 1.95 Å, and the R_{free} value was 25.1% (for 5% of the reflections not included in the refinement).

Finally, the *Mtb* AcpS model was evaluated with the program MolProbity.[45] The details of the refinement statistics of the AcpS structure are presented in Table 1. All figures depicting structures were prepared using PyMOL (DeLano Scientific LLC). Structure-based sequence alignment was performed using the program TCoffee.[34] The figure illustrating the structure-based sequence alignment was prepared using MultAlin[46] and ESPript.[35]

Accession number

The coordinates and structure factors for the *Mtb* AcpS structure have been deposited in the Research Collaboratory for Structural Bioinformatics PDB under accession no. 3HQJ.

Acknowledgements

We thank Prof. Joel Sussman and Dr. Virginia Buchner for helpful discussions. We thank Shoshana Tel-Or, Anna Branzburg, Reut Rotem Bernehim, David Marom, and Ada Dantes for their skilled assistance. The structure was determined at the Israel Structural Proteomics Center, supported by the Divadol Foundation, the European Commission Sixth Framework Research, and Technological Development Program contract no. 031220. This project was supported by the Israeli Ministry of Health Chief Scientist award no. 6223 (O.Z. and Y.B.). O.Z. was supported by a sabbatical fellowship from the Kimmelman Center for Macromolecular Structure and Assembly.

Supplementary Data

Supplementary data associated with this article can be found, in the online version, at doi:10.1016/j.jmb.2009.08.065

References

1. World Health Organization. (2007). WHO Tuberculosis World Health Organization. Geneva, Switzerland.
2. Glickman, M. S., Cox, J. S. & Jacobs, W. R., Jr (2000). A novel mycolic acid cyclopropane synthetase is required for cording, persistence, and virulence of *Mycobacterium tuberculosis*. *Mol. Cell*, **5**, 717–727.
3. Dao, D. N., Sweeney, K., Hsu, T., Gurcha, S. S., Nascimento, I. P., Roshevsky, D. *et al.* (2008). Mycolic acid modification by the mmaA4 gene of *M. tuberculosis* modulates IL-12 production. *PLoS Pathog.* **4**, e1000081.
4. Bhatt, A., Molle, V., Besra, G. S., Jacobs, W. R., Jr & Kremer, L. (2007). The *Mycobacterium tuberculosis* FAS-II condensing enzymes: their role in mycolic acid biosynthesis, acid-fastness, pathogenesis and in future drug development. *Mol. Microbiol.* **64**, 1442–1454.
5. Zhi, X. Y., Li, W. J. & Stackebrandt, E. (2009). An update of the structure and 16S rRNA gene sequence-based definition of higher ranks of the class Actinobacteria, with the proposal of two new suborders and four new families and emended descriptions of the existing higher taxa. *Int. J. Syst. Evol. Microbiol.* **59**, 589–608.
6. Schweizer, E. & Hofmann, J. (2004). Microbial type I fatty acid synthases (FAS): major players in a network of cellular FAS systems. *Microbiol. Mol. Biol. Rev.* **68**, 501–517.

7. Maier, T., Jenni, S. & Ban, N. (2006). Architecture of mammalian fatty acid synthase at 4.5 Å resolution. *Science*, **311**, 1258–1262.
8. Smith, S., Witkowski, A. & Joshi, A. K. (2003). Structural and functional organization of the animal fatty acid synthase. *Prog. Lipid Res.* **42**, 289–317.
9. White, S. W., Zheng, J., Zhang, Y. M. & Rock, C. O. (2005). The structural biology of type II fatty acid biosynthesis. *Annu. Rev. Biochem.* **74**, 791–831.
10. Cole, S. T., Brosch, R., Parkhill, J., Garnier, T., Churcher, C., Harris, D. *et al.* (1998). Deciphering the biology of *Mycobacterium tuberculosis* from the complete genome sequence. *Nature*, **393**, 537–544.
11. Kolattukudy, P. E., Fernandes, N. D., Azad, A. K., Fitzmaurice, A. M. & Sirakova, T. D. (1997). Biochemistry and molecular genetics of cell-wall lipid biosynthesis in mycobacteria. *Mol. Microbiol.* **24**, 263–270.
12. Butland, G., Peregrin-Alvarez, J. M., Li, J., Yang, W., Yang, X., Canadien, V. *et al.* (2005). Interaction network containing conserved and essential protein complexes in *Escherichia coli*. *Nature*, **433**, 531–537.
13. Byers, D. M. & Gong, H. (2007). Acyl carrier protein: structure–function relationships in a conserved multifunctional protein family. *Biochem. Cell Biol.* **85**, 649–662.
14. Lambalot, R. H., Gehring, A. M., Flugel, R. S., Zuber, P., LaCelle, M., Marahiel, M. A. *et al.* (1996). A new enzyme superfamily—the phosphopantetheinyl transferases. *Chem. Biol.* **3**, 923–936.
15. Mootz, H. D., Finking, R. & Marahiel, M. A. (2001). 4′-Phosphopantetheine transfer in primary and secondary metabolism of *Bacillus subtilis*. *J. Biol. Chem.* **276**, 37289–37298.
16. Parris, K. D., Lin, L., Tam, A., Mathew, R., Hixon, J., Stahl, M. *et al.* (2000). Crystal structures of substrate binding to *Bacillus subtilis* holo-(acyl carrier protein) synthase reveal a novel trimeric arrangement of molecules resulting in three active sites. *Structure*, **8**, 883–895.
17. Chirgadze, N. Y., Briggs, S. L., McAllister, K. A., Fischl, A. S. & Zhao, G. (2000). Crystal structure of *Streptococcus pneumoniae* acyl carrier protein synthase: an essential enzyme in bacterial fatty acid biosynthesis. *EMBO J.* **19**, 5281–5287.
18. Quadri, L. E., Weinreb, P. H., Lei, M., Nakano, M. M., Zuber, P. & Walsh, C. T. (1998). Characterization of Sfp, a *Bacillus subtilis* phosphopantetheinyl transferase for peptidyl carrier protein domains in peptide synthetases. *Biochemistry*, **37**, 1585–1595.
19. Mofid, M. R., Finking, R., Essen, L. O. & Marahiel, M. A. (2004). Structure-based mutational analysis of the 4′-phosphopantetheinyl transferases Sfp from *Bacillus subtilis*: carrier protein recognition and reaction mechanism. *Biochemistry*, **43**, 4128–4136.
20. Reuter, K., Mofid, M. R., Marahiel, M. A. & Ficner, R. (1999). Crystal structure of the surfactin synthetase-activating enzyme sfp: a prototype of the 4′-phosphopantetheinyl transferase superfamily. *EMBO J.* **18**, 6823–6831.
21. Leibundgut, M., Jenni, S., Frick, C. & Ban, N. (2007). Structural basis for substrate delivery by acyl carrier protein in the yeast fatty acid synthase. *Science*, **316**, 288–290.
22. Lomakin, I. B., Xiong, Y. & Steitz, T. A. (2007). The crystal structure of yeast fatty acid synthase, a cellular machine with eight active sites working together. *Cell*, **129**, 319–332.
23. Leibundgut, M., Maier, T., Jenni, S. & Ban, N. (2008). The multienzyme architecture of eukaryotic fatty acid synthases. *Curr. Opin. Struct. Biol.* **18**, 714–725.
24. Jenni, S., Leibundgut, M., Maier, T. & Ban, N. (2006). Architecture of a fungal fatty acid synthase at 5 Å resolution. *Science*, **311**, 1263–1267.
25. Fichtlscherer, F., Wellein, C., Mittag, M. & Schweizer, E. (2000). A novel function of yeast fatty acid synthase. Subunit alpha is capable of self-pantetheinylation. *Eur. J. Biochem.* **267**, 2666–2671.
26. Jenni, S., Leibundgut, M., Boehringer, D., Frick, C., Mikolasek, B. & Ban, N. (2007). Structure of fungal fatty acid synthase and implications for iterative substrate shuttling. *Science*, **316**, 254–261.
27. Chalut, C., Botella, L., de Sousa-D'Auria, C., Houssin, C. & Guilhot, C. (2006). The nonredundant roles of two 4′-phosphopantetheinyl transferases in vital processes of Mycobacteria. *Proc. Natl Acad. Sci. USA*, **103**, 8511–8516.
28. Kim, Y. & Prestegard, J. H. (1990). Refinement of the NMR structures for acyl carrier protein with scalar coupling data. *Proteins*, **8**, 377–385.
29. Xu, G. Y., Tam, A., Lin, L., Hixon, J., Fritz, C. C. & Powers, R. (2001). Solution structure of *B. subtilis* acyl carrier protein. *Structure*, **9**, 277–287.
30. Sharma, A. K., Sharma, S. K., Surolia, A., Surolia, N. & Sarma, S. P. (2006). Solution structures of conformationally equilibrium forms of holo-acyl carrier protein (PfACP) from *Plasmodium falciparum* provides insight into the mechanism of activation of ACPs. *Biochemistry*, **45**, 6904–6916.
31. Cryle, M. J. & Schlichting, I. (2008). Structural insights from a P450 Carrier Protein complex reveal how specificity is achieved in the P450(BioI) ACP complex. *Proc. Natl Acad. Sci. USA*, **105**, 15696–15701.
32. Roujeinikova, A., Simon, W. J., Gilroy, J., Rice, D. W., Rafferty, J. B. & Slabas, A. R. (2007). Structural studies of fatty acyl-(acyl carrier protein) thioesters reveal a hydrophobic binding cavity that can expand to fit longer substrates. *J. Mol. Biol.* **365**, 135–145.
33. Wong, H. C., Liu, G., Zhang, Y. M., Rock, C. O. & Zheng, J. (2002). The solution structure of acyl carrier protein from *Mycobacterium tuberculosis*. *J. Biol. Chem.* **277**, 15874–15880.
34. Armougom, F., Moretti, S., Poirot, O., Audic, S., Dumas, P., Schaeli, B. *et al.* (2006). Expresso: automatic incorporation of structural information in multiple sequence alignments using 3D-Coffee. *Nucleic Acids Res.* **34**, W604–W608.
35. Gouet, P., Courcelle, E., Stuart, D. I. & Metoz, F. (1999). ESPript: analysis of multiple sequence alignments in PostScript. *Bioinformatics*, **15**, 305–308.
36. Holm, L., Kaariainen, S., Rosenstrom, P. & Schenkel, A. (2008). Searching protein structure databases with DaliLite v.3. *Bioinformatics*, **24**, 2780–2781.
37. Bunkoczi, G., Pasta, S., Joshi, A., Wu, X., Kavanagh, K. L., Smith, S. & Oppermann, U. (2007). Mechanism and substrate recognition of human holo ACP synthase. *Chem. Biol.* **14**, 1243–1253.
38. Wallace, A. C., Laskowski, R. A. & Thornton, J. M. (1995). LIGPLOT: a program to generate schematic diagrams of protein–ligand interactions. *Protein Eng.* **8**, 127–134.
39. Gilbert, A. M., Kirisits, M., Toy, P., Nunn, D. S., Failli, A., Dushin, E. G. *et al.* (2004). Anthranilate 4*H*-oxazol-5-ones: novel small molecule antibacterial acyl carrier protein synthase (AcpS) inhibitors. *Bioorg. Med. Chem. Lett.* **14**, 37–41.
40. Joseph-McCarthy, D., Parris, K., Huang, A., Failli, A., Quagliato, D., Dushin, E. G. *et al.* (2005). Use of

structure-based drug design approaches to obtain novel anthranilic acid acyl carrier protein synthase inhibitors. *J. Med. Chem.* **48**, 7960–7969.
41. Otwinowski, Z. & Minor, W. (1997). Processing of X-ray diffraction data collected in oscillation mode. *Methods Enzymol.* **276**, 307–326.
42. French, G. S. & Wilson, K. S. (1978). On the treatment of negative intensity observations. *Acta Crystallogr., Sect. A: Cryst. Phys., Diffr., Theor. Gen. Crystallogr.* **34**, 517–552.
43. Murshudov, G. N., Vagin, A. A. & Dodson, E. J. (1997). Refinement of macromolecular structures by the maximum-likelihood method. *Acta Crystallogr., Sect. D: Biol. Crystallogr.* **53**, 240–255.
44. Emsley, P. & Cowtan, K. (2004). Coot: model-building tools for molecular graphics. *Acta Crystallogr., Sect. D: Biol. Crystallogr.* **60**, 2126–2132.
45. Davis, I. W., Leaver-Fay, A., Chen, V. B., Block, J.N., Kapral, G. J., Wang, X. *et al.* (2007). MolProbity: all-atom contacts and structure validation for proteins and nucleic acids. *Nucleic Acids Res.* **35**, W375–W383.
46. Corpet, F. (1988). Multiple sequence alignment with hierarchical clustering. *Nucleic Acids Res.* **16**, 10881–10890.